Supporting Information for

Li^+ intercalated $V_2O_5 \cdot nH_2O$ with enlarged layer spacing and fast ion diffusion as an aqueous zinc-ion battery cathode

Yongqiang Yang,[a] Yan Tang,[a,b] Guozhao Fang,[a] Lutong Shan,[a] Jiasheng Guo,[a] Wenyu Zhang,[a] Chao Wang,[c] Liangbing Wang,[a,b] Jiang Zhou,[a,b,*] and Shuquan Liang[a,b,*]

a. School of Materials Science and Engineering, Central South University, Changsha 410083, P. R. China. zhou_jiang@csu.edu.cn, lsq@csu.edu.cn

b. Key Laboratory of Nonferrous Metal Materials Science and Engineering, Ministry of Education, Central South University, Changsha 410083, Hunan, China.

c Department of Nuclear Science and Engineering, Massachusetts Institute of Technology, Cambridge, Massachusetts 02139, United States.

Experimental Section

Synthesis

Typically, 0.3 g V_2O_5 were dissolved in 30 mL of deionized water with 4 mL H_2O_2 added dropwise. After stirring at 40°C for 30 min, 22.7 mg $LiNO_3$ (V_2O_5 and $LiNO_3$ in a stoichiometric ratio of 1:0.1) was added into the orange solution followed by continuously stirring for another 30 min. Afterwards, the mixed solution was transferred into a 50 mL Teflon-lined autoclave and maintained at 200°C for 48 h. LVO was obtained after centrifuged several times with alcohol and dried. Meanwhile, the LVO-200/250/300 were prepared by annealing LVO at 200/250/300°C for 2 h with a heating rate of 2°C min^{-1} in air.

In addition, VO-250 for comparison was synthesized by the same experimental parameters without adding the $LiNO_3$.

Material characterizations

The crystallographic phases of samples were determined by a Rigaku D/max 2500 X-ray powder diffractometer with Cu Kα-radiation (λ = 0.15405 nm). The morphologies were characterized by scanning electron microscopy (SEM, FEI Nova NanoSEM 230m, 10 kV) and transmission electron microscopy (TEM, Titan G2 60-300) was performed to scan High-resolution TEM (HRTEM) images, selected area electron diffraction (SAED) patterns and energy dispersive spectrometer (EDS) mappings for further investigation of structural characterization. ESCALAB 250 Xi X-ray photoelectron spectrometer (Thremo Fisher) was used to measure the XPS spectra. The thermogravimetric analysis (TGA) under argon atmosphere was collected by thermal gravimetric analyzer (NETZSCH STA 449C).

Electrochemical measurements

The electrochemical measurements of the composites were investigated via stain-less coin cells (CR2016) which were assembled in air. The electrode was prepared by coating a slurry mixed the composites, acetylene black and Poly(vinylidene fluoride) (PVDF) with the mass ratio of 7:2:1 onto a stainless-steel mesh and dried in a vacuum oven at 80°C for 12 h (SEM images of the electrode film are shown in Fig. S4, SI). Metallic zinc plates and glass fiber were used as anode and separator, respectively as well as 2 M zinc sulfate ($ZnSO_4$) solution was used as the electrolyte.

The electrochemical performances of the coin cells were measured in a potential range of 0.4 -1.4 V (*vs.* Zn^{2+}/Zn) utilizing a multichannel battery test system (Land CT 2001A). CV curves (0.4 -1.4 V *vs.* Zn^{2+}/Zn) and electrochemical impedance spectrometry (EIS) from 100 kHz to 10 mHz were carried out using an electrochemical workstation (MULTI AUTOLAB M204, Metrohm). The areal loading of composites for each electrode in this work is about 0.9-1.2 mg/cm^2, except that in Fig. S8 (SI) is ~2.8 mg/cm^2.

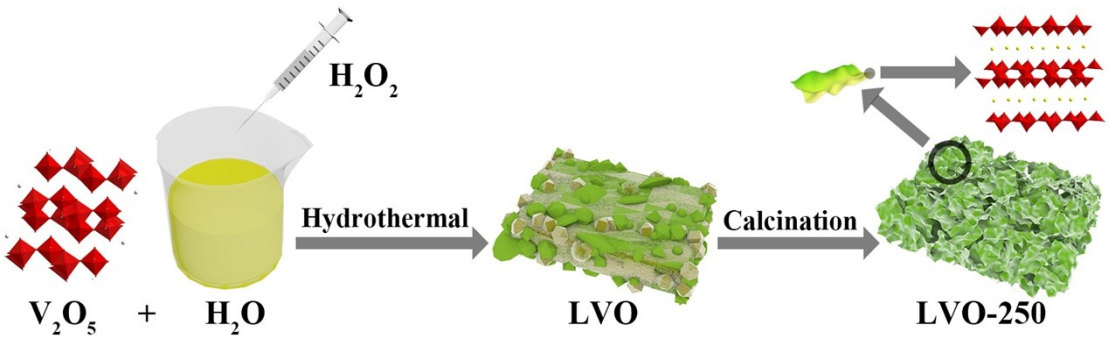

Figure S1. Illustration of synthesis process of LVO and cotton-like LVO-250.

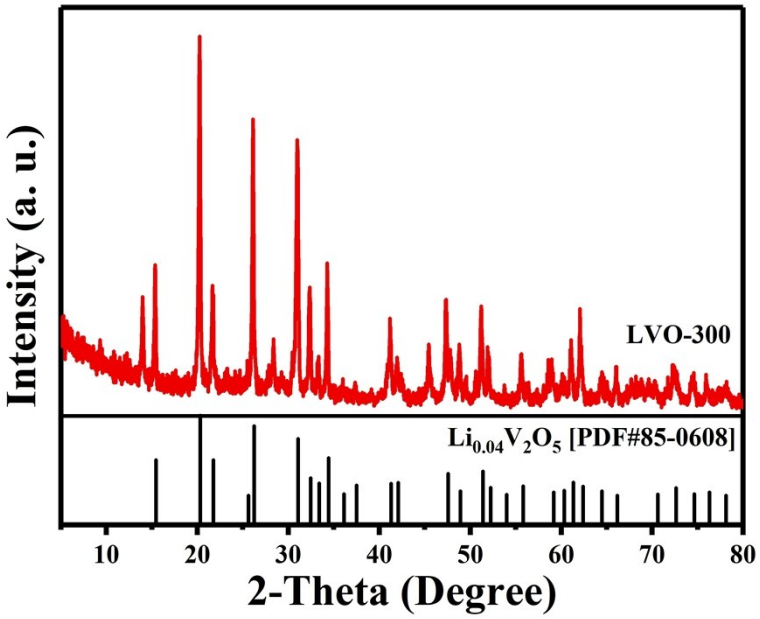

Figure S2. XRD pattern of LVO-300.

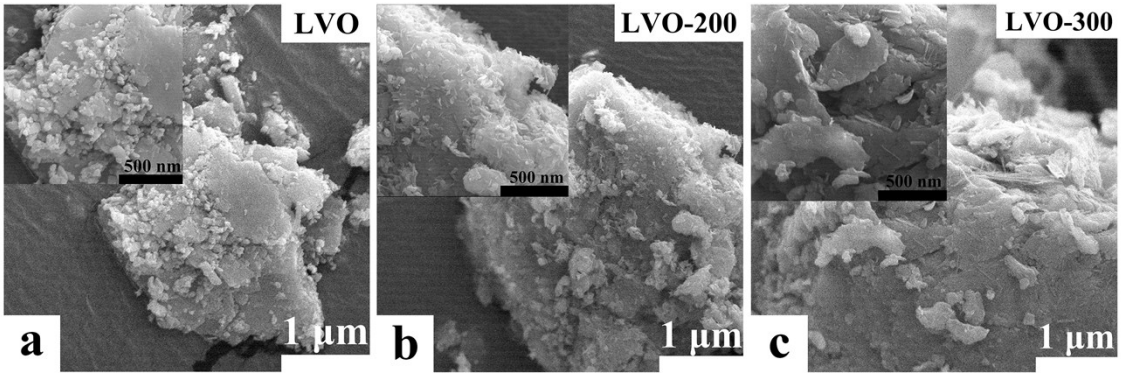

Figure S3. SEM images of a) LVO, b) LVO-200 and c) LVO-300.

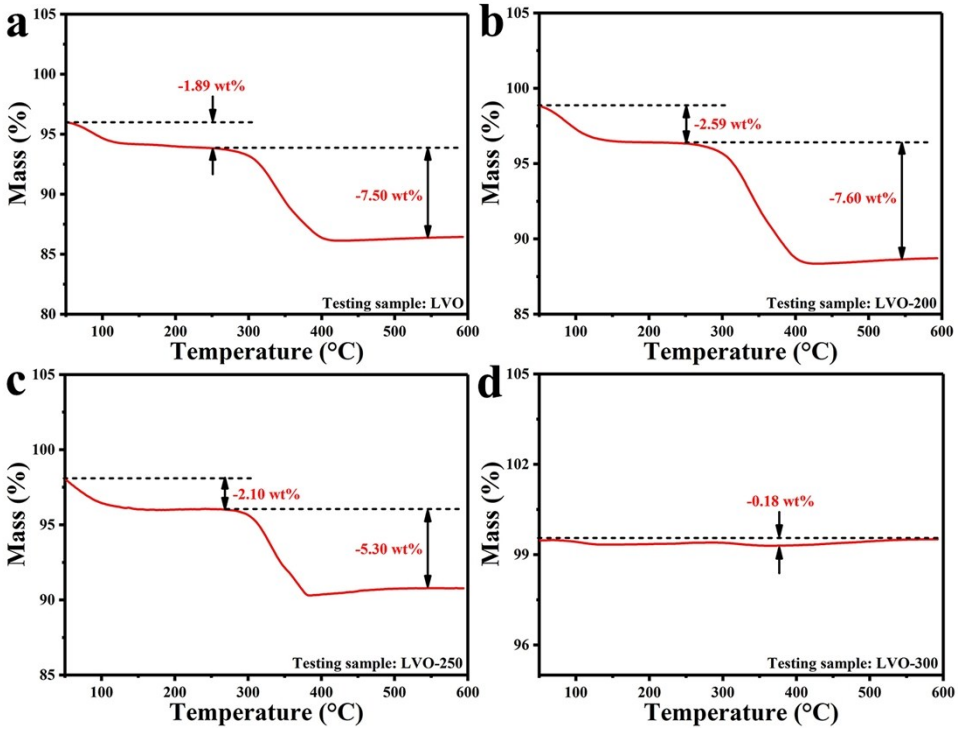

Figure S4. TGA results of LVO-0/200/250/300 in argon atmosphere, respectively.

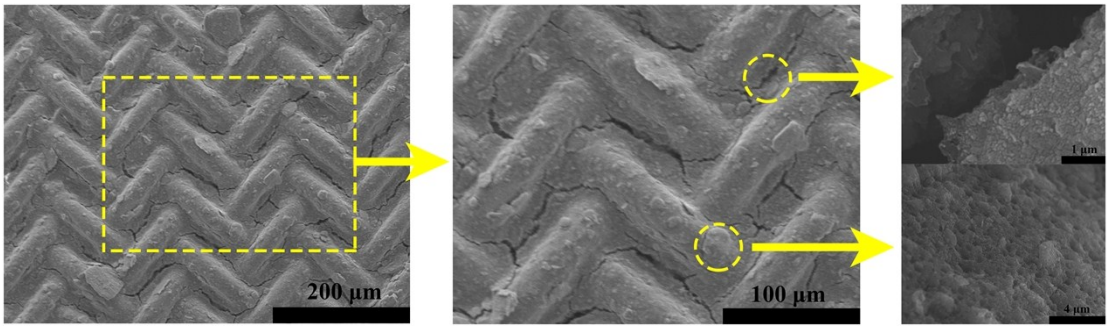

Figure S5. SEM images with different magnifications of LVO-250 electrode film.

It can be observed from the images of electrode film that the mixture of LVO-250 sample and acetylene black uniformly attached to the surface of stainless steel mesh. Furthermore, the high resolution image of the surface and cross-section of electrode also reflected that the surface and internal structure of the mixture are relatively loose.

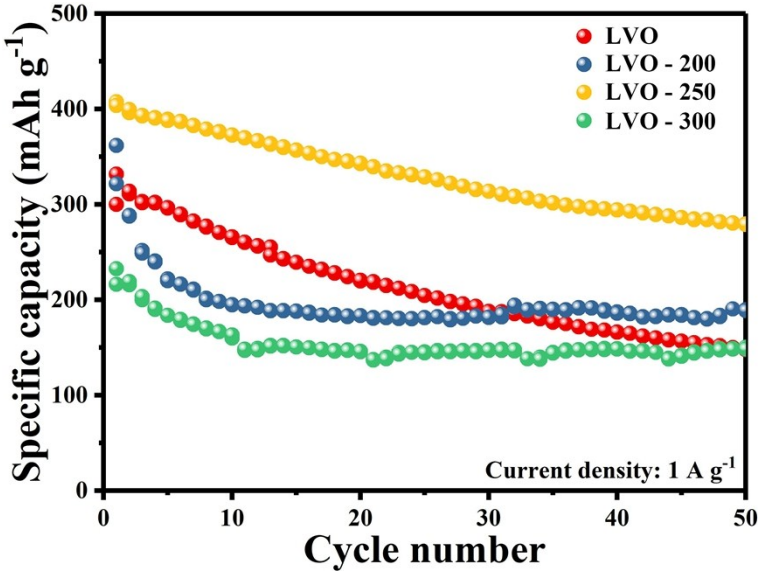

Figure S6. Cycling performances of LVO and LVO-200/250/300 at current density of 1 A g^{-1}.

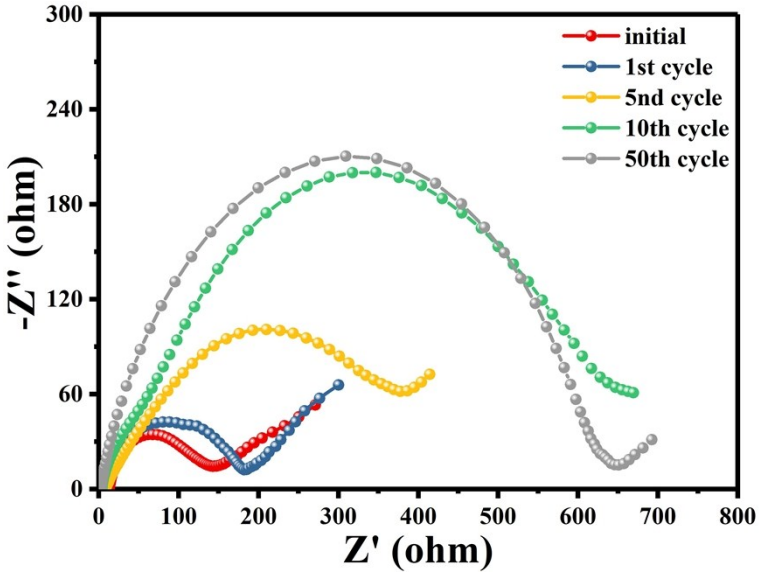

Figure S7. The electrochemical impedance spectra (EIS) of LVO-250 electrodes in the initial state, after 1st, 5th, 10th, and 50th cycles.

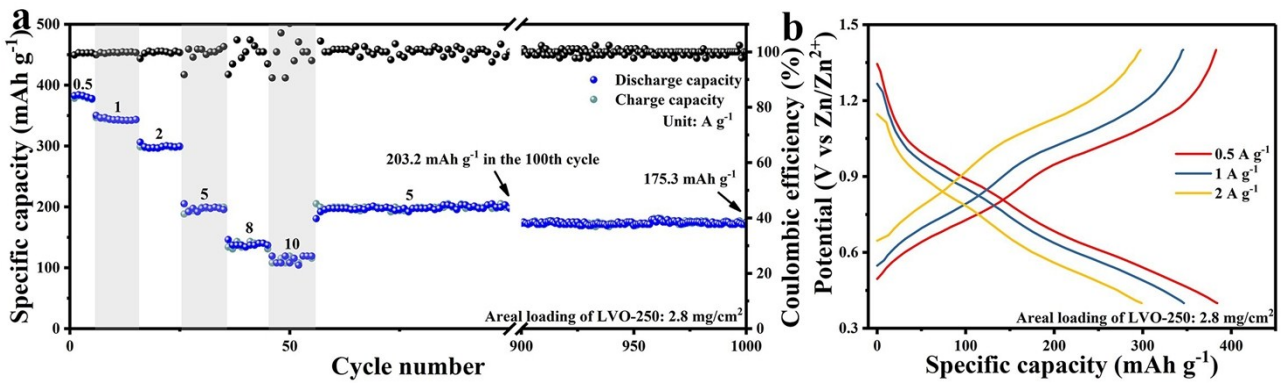

Figure S8. a) Rate capacities at the current densities between 0.5 to 10 A g^{-1} followed by long cycling performance at 5 A g^{-1} and b) representative galvanostatic charge-discharge (GCD) curves of LVO-250 electrode with higher areal loading.

When the loading of LVO-250 composite reaches to ~2.8 mg/cm^2, the electrode still delivers a favorite rate capacity with average discharge capacities of 382, 344, 299, 197, 138 and 114 mA h g^{-1} at the current densities of 0.5, 1, 2, 5, 8 and 10 A g^{-1}, respectively. Furthermore, high discharge capacities of 192, 203 and 175 mA h g^{-1} after 1, 100 and 1000 cycles can be observed while the current density returning to 5 A g^{-1}, respectively.

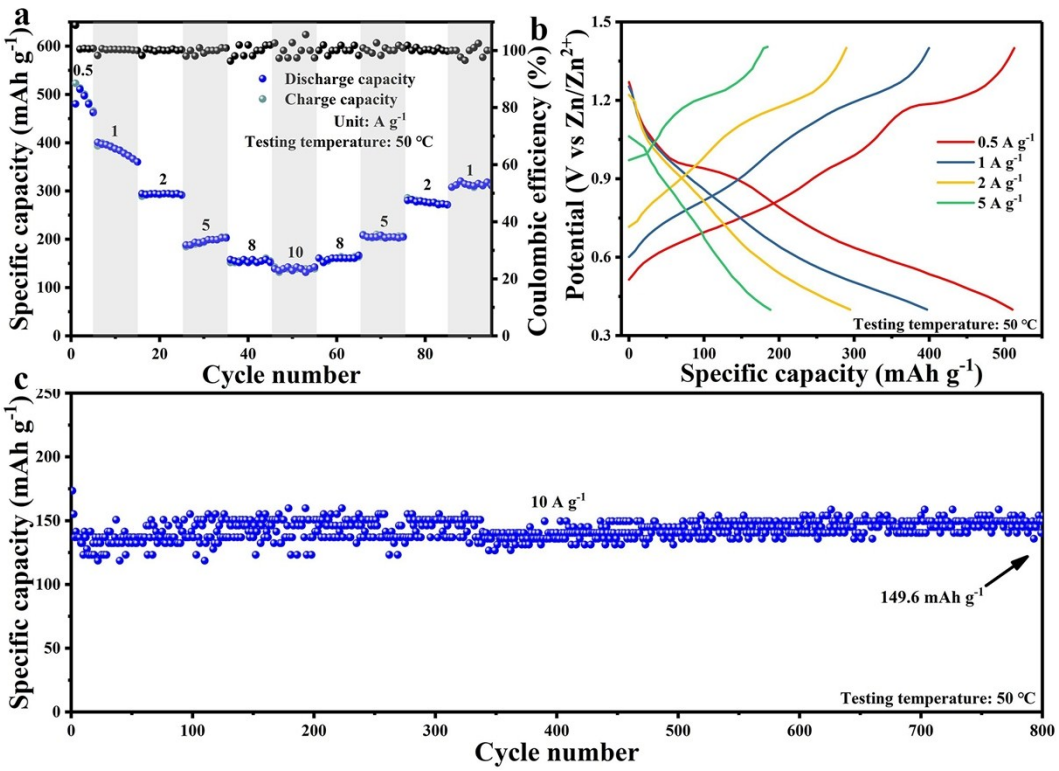

Figure S9. a) Rate capacities at current densities between 0.5 to 10 A g^{-1}, b) representative GCD curves and c) cycling performance at 10 A g^{-1} at 50°C of LVO-250 sample.

The LVO-250 electrode delivers average discharge capacities of 486, 383, 294, 196, 155 and 139 mA h g^{-1} at the current densities of 0.5, 1, 2, 5, 8 and 10 A g^{-1} at the testing temperature of 50°C, respectively, with stable charging/discharging voltage platforms.

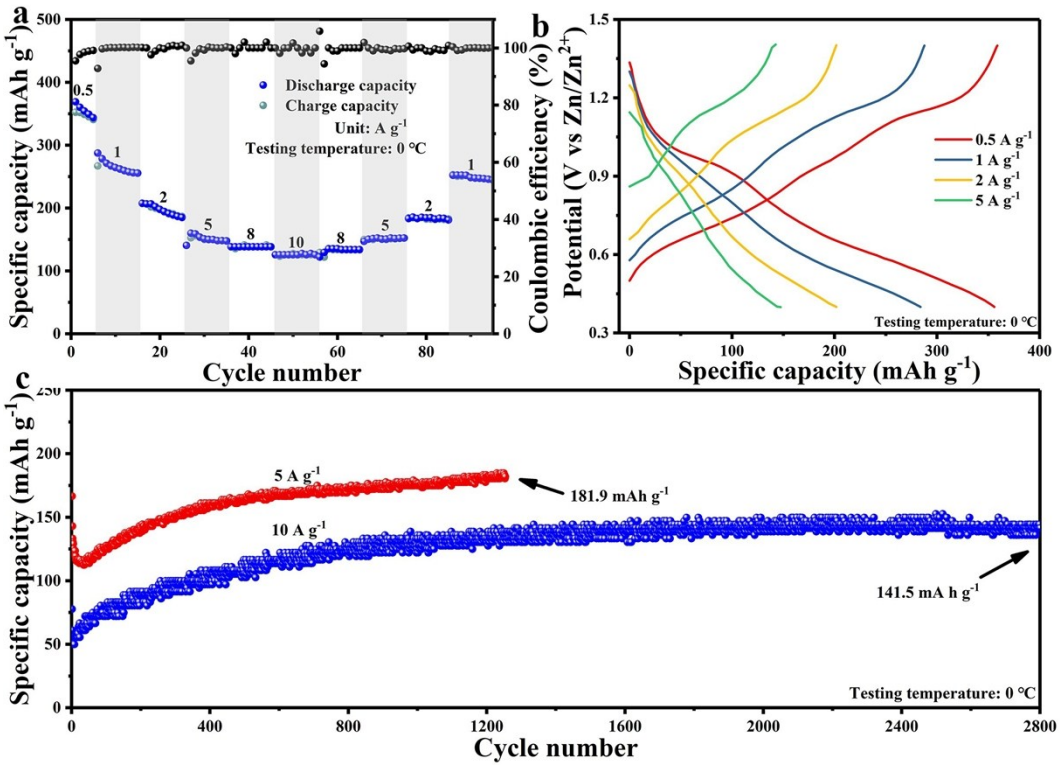

Figure S10. a) Rate capacities at current densities between 0.5 to 10 A g^{-1}, b) representative GCD curves and c) cycling performance at 5, 10 A g^{-1} at 0°C of LVO-250 sample.

The LVO-250 electrode delivers average discharge capacities of 355, 266, 197, 151, 138 and 126 mA h g^{-1} at the current densities of 0.5, 1, 2, 5, 8 and 10 A g^{-1} at the testing temperature of 0°C, respectively, with stable charging/discharging voltage platforms.

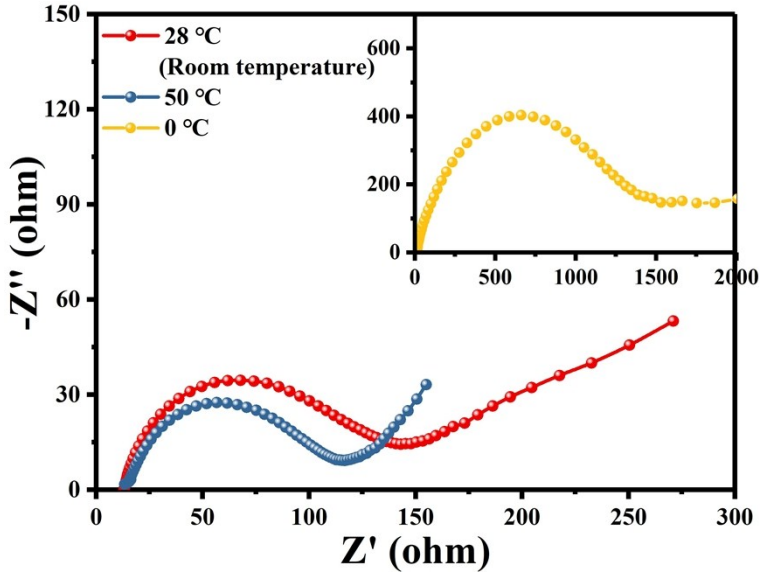

Figure S11. The EIS plots of LVO-250 electrode in the testing temperatures of 0, 28 (room temperature) and 50°C.

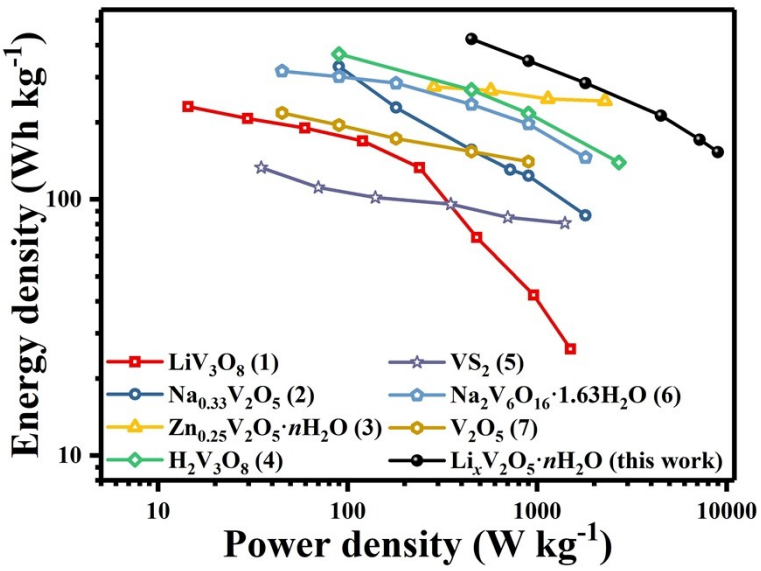

Figure S12. Comparison of energy and power densities of LVO-250 cathode with the reported cathodes in aqueous ZIBs (e.g. LiV_3O_8,[1] $Na_{0.33}V_2O_5$,[2] $Zn_{0.25}V_2O_5{\cdot}nH_2O$,[3] $H_2V_3O_8$,[4] VS_2,[5] $Na_2V_6O_{16}{\cdot}nH_2O$[6] and V_2O_5[7]).

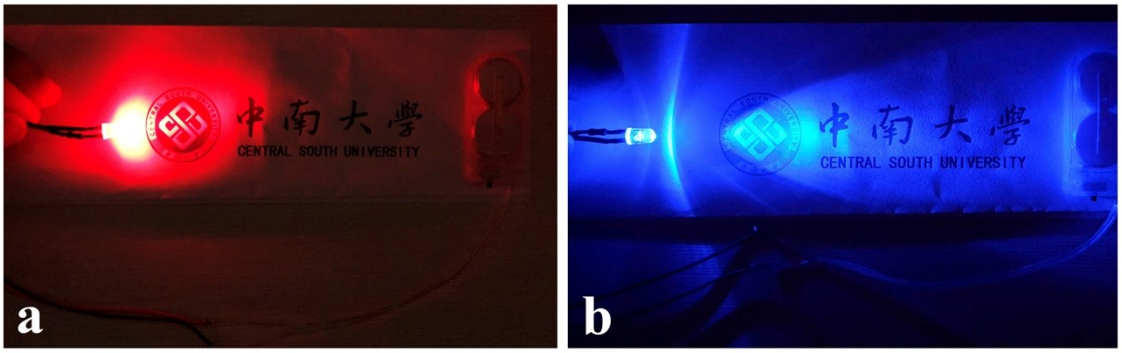

Figure S13. a) Red and b) blue lamp beads lightened by four coin cells using LVO-250 electrode.

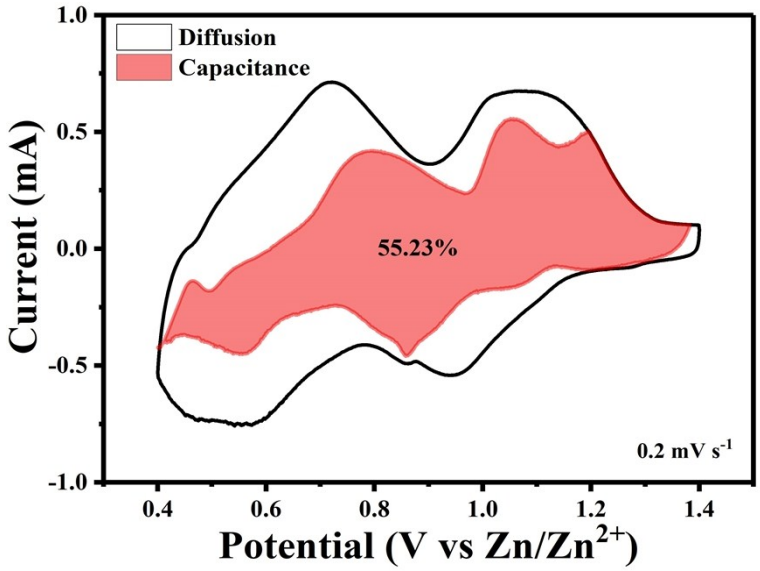

Figure S14. Pseudocapacitive fraction (shown by the shaded area) calculated at a scan rate of 0.2 mV s^{-1} from CV curves at different scan rates.

According to the work of Dunn[8], the measure current (i) and scan rate (v) in CV curves have relationships with equation:

$$i = av^b$$

$$log(i) = b \times log(v) + log(a)$$

Where a, b are adjustable parameters in which the value of b is between 0.5 and 1, in which the b value of 0.5 indicates a full diffusion-controlled process and b = 1 corresponds to the full capacitive contribution. The values of b can be obtained by calculating the slope of the *-log(i) vs. -log(v)* plots. Meanwhile, the contribution of pseudocapacitive can be quantified by the equations:[8-10]

$$i = k_1v + k_2v^{1/2}$$

$$i/v^{1/2} = k_1v^{1/2} + k_2$$

Where the capacitive contribution can be divided into capacitive (measured with k_1) and diffusion-controlled (measured with k_2). By determining values of both k_1 and k_2, we can distinguish the fraction of the current from surface capacitance and diffusion limitted.[5]

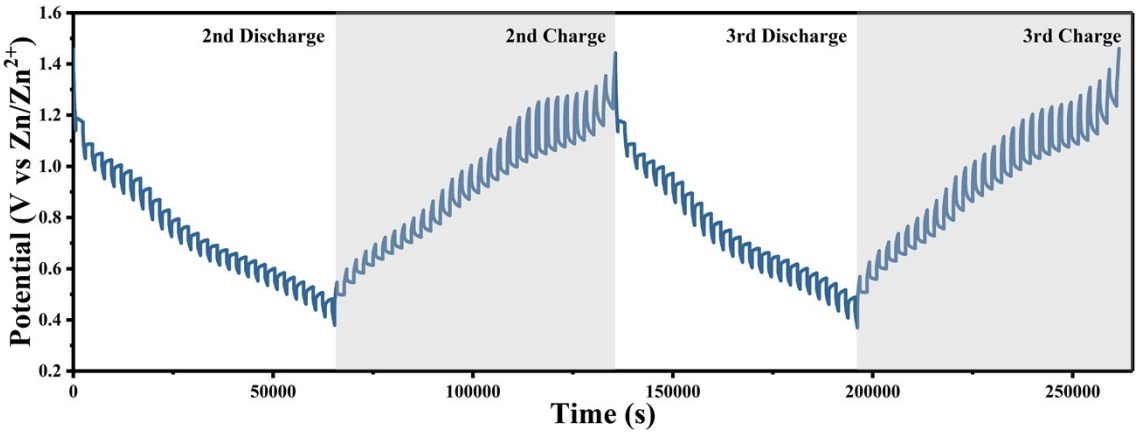

Figure S15. The discharge/charge GITT curves of VO-250 electrode in the 2nd and 3rd cycles.

The diffusion coefficient of Zn^{2+} was measured by using Ganlvanostatic Intermittent Titration Technique (GITT) and calculated based on the following equation:[11-14]

$$D = \frac{4L^2}{\pi\tau}\left(\frac{\Delta E_S}{\Delta E_t}\right)^2$$

Where t and τ represent the duration of current pulse (s) and relaxation time (s), respectively. L corresponds to Zn^{2+} diffusion length, which is equal to thickness of electrode. ΔE_S and ΔE_t are the steady-state voltage change (V) by the current pulse and voltage change (V) during the constant current pulse (eliminating the voltage changes after relaxation time).

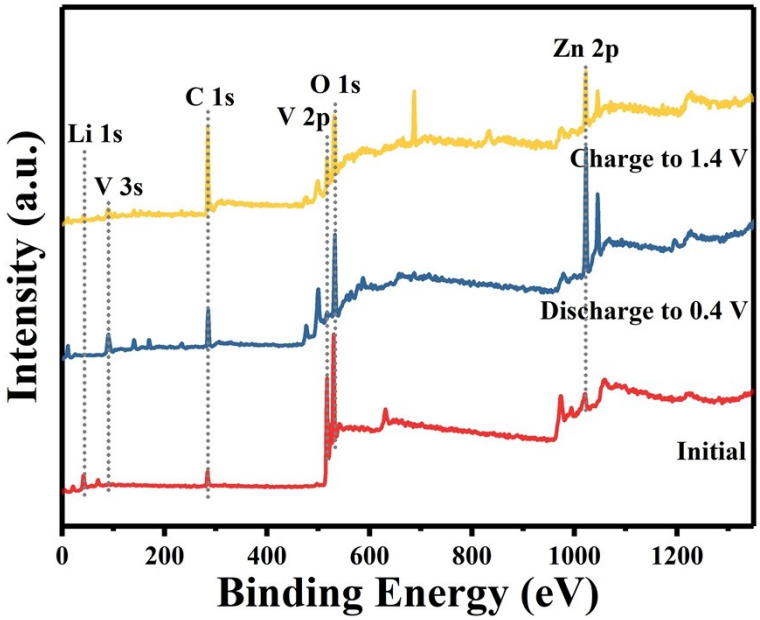

Figure S16. XPS spectra at the pristine, fully discharged and charged states of LVO-250, respectively.

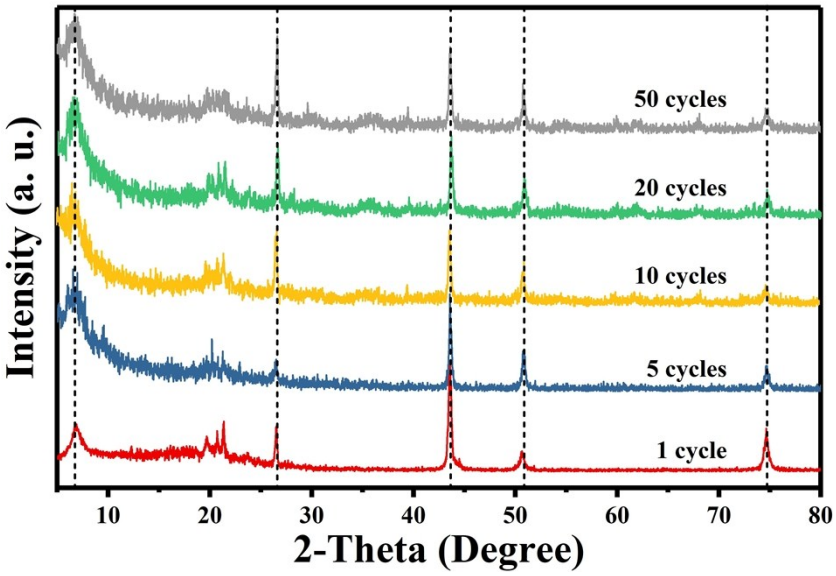

Figure S17. XRD patterns of electrode after 1st, 5th, 10th, 20th and 50th cycles, respectively.

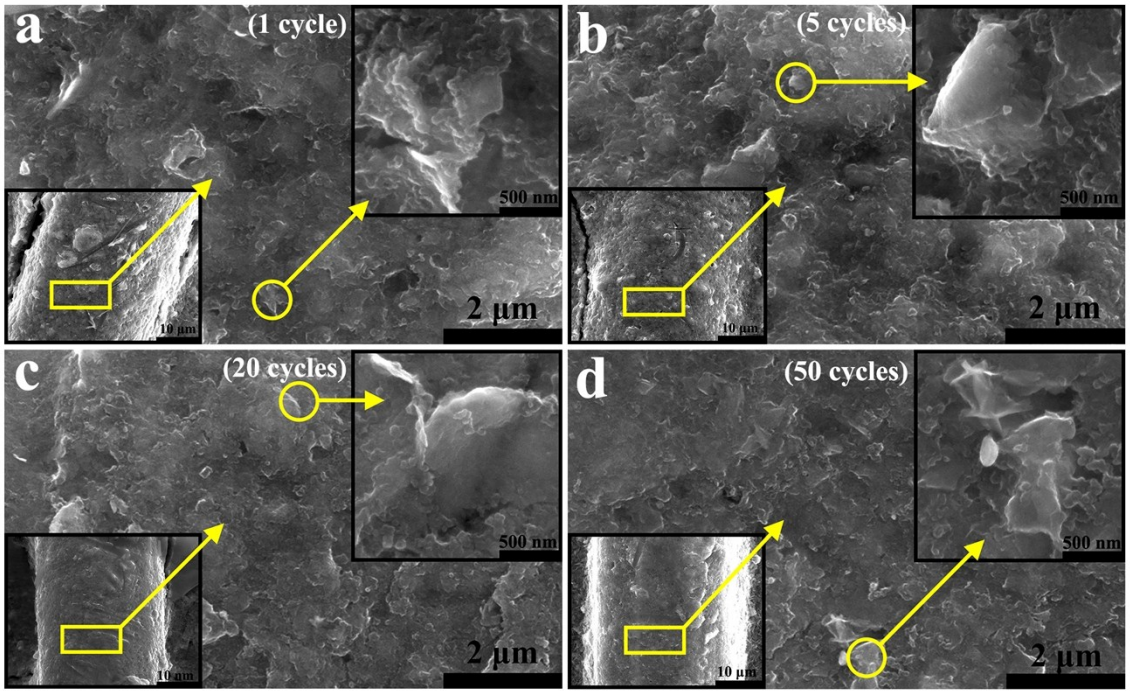

Figure S18. SEM images of electrode after 1st, 5th, 20th and 50th cycles, respectively.

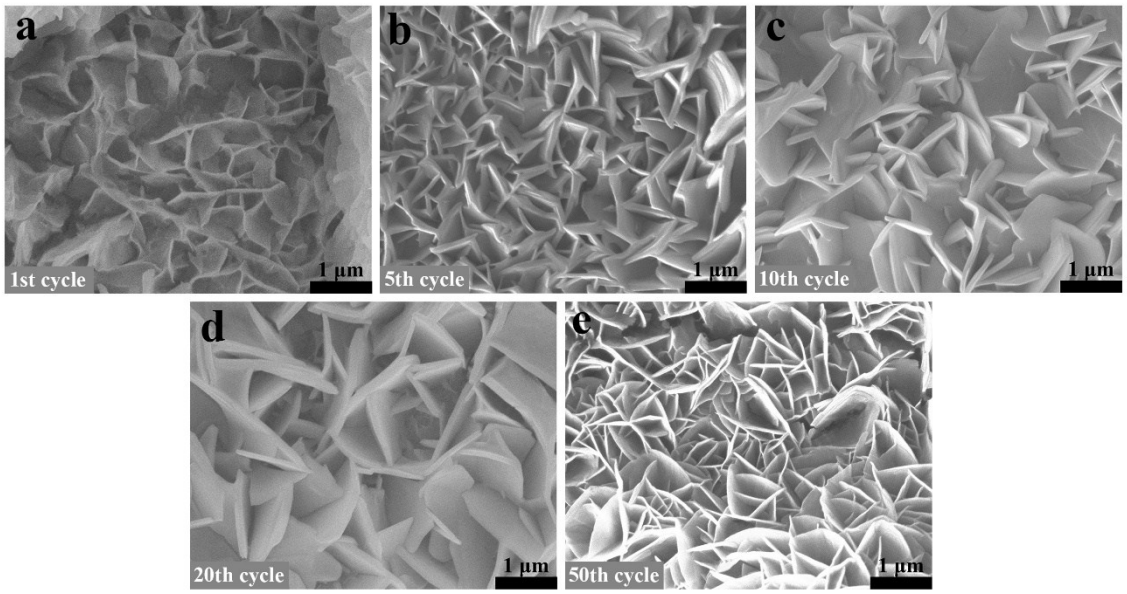

Figure S19. SEM images of Zn anode after a) 1st, b) 5th, c) 10th, d) 20th and e) 50th cycles, respectively.

Notes and references

1. M. H. Alfaruqi, V. Mathew, J. Song, S. Kim, S. Islam, D. T. Pham, J. Jo, S. Kim, J. P. Baboo, Z. Xiu, K.-S. Lee, Y.-K. Sun and J. Kim, *Chem. Mater.*, 2017, **29**, 1684-1694.
2. P. He, G. B. Zhang, X. B. Liao, M. Y. Yan, X. Xu, Q. Y. An, J. Liu and L. Q. Mai, *Adv. Energy Mater.*, 2018, **8**, 1702463.
3. D. Kundu, B. D. Adams, V. Duffort, S. H. Vajargah and L. F. Nazar, *Nat. Energy*, 2016, **1**, 16119.
4. P. He, Y. Quan, X. Xu, M. Yan, W. Yang, Q. An, L. He and L. Mai, *Small*, 2017, **13**, 1702551.
5. P. He, M. Yan, G. Zhang, R. Sun, L. Chen, Q. An and L. Mai, *Adv. Energy Mater.*, 2017, **7**, 1601920.
6. P. Hu, T. Zhu, X. Wang, X. Wei, M. Yan, J. Li, W. Luo, W. Yang, W. Zhang, L. Zhou, Z. Zhou and L. Mai, *Nano Lett.*, 2018, **18**, 1758-1763.
7. P. Hu, M. Yan, T. Zhu, X. Wang, X. Wei, J. Li, L. Zhou, Z. Li, L. Chen and L. Mai, *ACS Appl. Mater. Inter.*, 2017, **9**, 42717-42722.
8. J. P. John Wang, James Lim, and Bruce Dunn, *J. Phys. Chem. C*, 2007, **111**, 14925-14931.
9. T. Brezesinski, J. Wang, S. H. Tolbert and B. Dunn, *Nat. Mater.*, 2010, **9**, 146-151.
10. D. Chao, C. Zhu, P. Yang, X. Xia, J. Liu, J. Wang, X. Fan, S. V. Savilov, J. Lin, H. J. Fan and Z. X. Shen, *Nat. Commun.*, 2016, **7**, 12122.
11. A. K. Jordan Anderson, Diego J. Dı ´az and Sudipta Seal, *J. Phys. Chem. C*, 2010, **114**, 4595–4602.
12. B. A. B. a. R. A. H. C. JohnWen, *J. Electrochem. Soc.*, 1979, **126**, 2258-2266.
13. W. W. a. R. A. Huggins, *J. Electrochem. Soc.*, 1977, **124**, 1569-1577.
14. D. T. Ngo, H. T. T. Le, C. Kim, J.-Y. Lee, J. G. Fisher, I.-D. Kim and C.-J. Park, *Energy Environ. Sci.*, 2015, **8**, 3577-3588.